CHEMICAL PHYSICS

Direct quantitative measurement of the C=O···H–C bond by atomic force microscopy

Shigeki Kawai,[1,2,3]* Tomohiko Nishiuchi,[4] Takuya Kodama,[4] Peter Spijker,[5] Rémy Pawlak,[2] Tobias Meier,[2] John Tracey,[5] Takashi Kubo,[4] Ernst Meyer,[2] Adam S. Foster[5,6]*

The hydrogen atom—the smallest and most abundant atom—is of utmost importance in physics and chemistry. Although many analysis methods have been applied to its study, direct observation of hydrogen atoms in a single molecule remains largely unexplored. We use atomic force microscopy (AFM) to resolve the outermost hydrogen atoms of propellane molecules via very weak C=O···H–C hydrogen bonding just before the onset of Pauli repulsion. The direct measurement of the interaction with a hydrogen atom paves the way for the identification of three-dimensional molecules such as DNAs and polymers, building the capabilities of AFM toward quantitative probing of local chemical reactivity.

INTRODUCTION

With just a single electron and a single proton, hydrogen is the smallest atom, yet its generation in the early stages of the universe makes it the most abundant element, constituting 75% of all baryonic mass. The extremely high reactivity of hydrogen means it easily forms covalent compounds with nearly all nonmetallic elements, famously, oxygen and carbon. Hence, identifying and understanding the role of such a ubiquitous element have long been key scientific challenges. In particular, hydrocarbons are one of the most varied and functionalized products at the heart of engineering, chemistry, and life, and hydrogen is often critical in their function.

In general, to investigate the molecular structure in a crystal, analyses by infrared spectroscopy, nuclear magnetic resonance spectroscopy, and x-ray crystallography are commonly used. These offer varying sensitivity to molecular structure, and the presence of hydrogen is generally particularly difficult to establish. Recent improvements in scanning transmission electron microscopy (STEM), namely, aberration correction (*1*), allow us to see individual atoms in thin films, and even hydrogen atoms in the crystalline solid YH_2 can be resolved by annular bright-field imaging (*2*). However, for molecules, electron irradiation with high energy strongly limits the resolution, with only rare examples of the observation of small molecular clusters (*3*). Thus, the observation of hydrogen atoms in a single molecule via STEM has yet to be achieved.

In contrast, the strong charge redistribution induced by hydrogenation is readily detectable in scanning tunneling microscopy (STM) measurements. Even in the early years of the technique, hydrogen adsorbed on a Si(100) surface was observed via the modulated electronic state of the hydrides (*4*). Later studies looked intensively into the chemistry of hydrogen in molecules (*5*–*11*), including detection of the vibration of the C–H bond via inelastic tunneling current (*12*) and of the spin-split state induced by the C–H bond on graphene (*13*). Although these studies paved the way for molecular chemistry and engineering, the long range of the molecular orbitals prevents the direct observation of a hydrogen atom in molecules. In atomic force microscopy (AFM), chemical reactivity has been explored in pioneering work on silicon surfaces (*14*, *15*), but extending this to molecules and quantitative bond studies still required innovations in functionalized tip imaging (*16*). This offers a tool to finally image internal molecular structure because the onset of the Pauli repulsion and the flexibility of a CO-functionalized tip offer a highly local probe of chemical reactivity (*17*), with the promise of directly studying the bonding of hydrogen. Recently, there have been several breakthrough studies of molecular characterization using functionalized AFM (*18*–*22*), but as yet, observed molecules on surfaces are usually planar and the tip-molecule junction of C=O···H–C has never been investigated systematically.

Here, we present the ability of high-resolution AFM to resolve the hydrogen atoms and interactions in carefully chosen configurations of three-dimensional hydrocarbons based on propellane derivatives. The hydrogen atoms located topmost in two stable adsorption configurations were directly observed by detecting the C=O···H–C hydrogen bonding. Our density functional theory (DFT) calculations confirm the signature of directional bonding, characteristic of very weak hydrogen bonding.

RESULTS

Pentacene is a planar aromatic molecule that was first used in the context of high-resolution AFM to observe intramolecular bonding (*16*). Here, the C–H bonds were also resolved, demonstrating significantly weaker contrast than the C–C bonds. Similar to the C–H bond, the C–F bond in fluoro-substituted aromatic molecules has also been resolved (*23*–*25*). The contrast of the C–F bond is stronger than that of the C–H because of the larger total charge density of the sigma bond and/or the larger potential depth of the fluorine atom (*25*). However, for planar molecules adsorbed on flat surfaces, part of the success of CO-functionalized tips is the enhanced contrast due to the tilting of the CO molecule because it deflects to trace the landscape of the tip-surface energy potential (*26*). This has even resulted in mistaken assignment of apparent bonds in images where they should not be physically present (*27*, *28*), further complicating the interpretation of high-resolution images. Even in the case where bond assignment is straightforward, the AFM is resolving the bonds, instead of the carbon, hydrogen, or fluorine atoms themselves. A strategy to overcome this challenge is to engineer a system where the C–H bond would point out perpendicular from the surface, offering the possibility to unambiguously resolve the hydrogen atom in

[1]International Center for Materials Nanoarchitectonics, National Institute for Materials Science, 1-1 Namiki, Tsukuba, Ibaraki 305-0044, Japan. [2]Department of Physics, University of Basel, Klingelbergstrasse 82, CH-4056 Basel, Switzerland. [3]Precursory Research for Embryonic Science and Technology, Japan Science and Technology Agency, 4-1-8 Honcho, Kawaguchi, Saitama 332-0012, Japan. [4]Department of Chemistry, Graduate School of Science, Osaka University, Toyonaka, Osaka 560-0043, Japan. [5]Centre of Excellence in Computational Nanoscience, Department of Applied Physics, Aalto University, PO Box 11100, FI-00076 Aalto, Finland. [6]Division of Electrical Engineering and Computer Science, Kanazawa University, Kanazawa 920-1192, Japan.
*Corresponding author. Email: shigeki.kawai@unibas.ch (S.K.); adam.foster@aalto.fi (A.S.F.)

a single molecule. For this reason, we used trinaphtho[3.3.3]propellane (TNP) (Fig. 1A) and trifluorantheno[3.3.3]propellane (TFAP) molecules (Fig. 1B) in this study (*29*, *30*). They adsorb to the substrate in either the upright (as shown in Fig. 1, top panel) or side-lying (Fig. 1, bottom panel) configuration, with the three-dimensional hydrocarbons at the center, ensuring that C–H bonds are always pointing outward.

Short one-dimensional structures were observed in STM topography when a small amount of TNP was deposited on a clean Ag(111) surface (Fig. 2A). The ends of the structures generally appear semispherical, whereas some appear as simple oval-like at a low bias voltage (fig. S1).

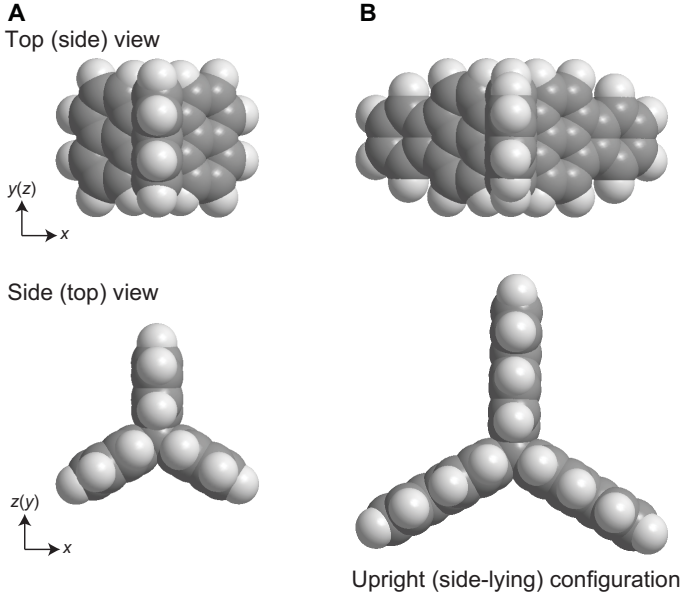

Fig. 1. Chemical structures. (**A**) TNP (*29*, *30*) and (**B**) TFAP. The top panel shows the top (side) view, and the bottom panel shows the side (top) view for the upright (side-lying) configuration.

Counting these shapes, we found that most of them are composed of TNPs, up to a maximum of a pentamer assembly (Fig. 2A, inset). To analyze the configuration in detail, we switched to AFM using a CO-functionalized tip (*16*) and observed the dimer TNPs, as indicated by a dashed box in Fig. 2A. Figure 2B shows the corresponding AFM image, in which two bright spots appear in each molecule, as indicated by red arrows and ovals. Assuming that the contrast relates to the hydrogen atoms, we can conclude that the TNPs are adsorbed as upright. The repulsion between hydrogen atoms in the adjacent TNPs induces the lateral shift in the condensation (fig. S2). An increase in the number of deposited TNPs results in the appearance of larger one-dimensional chain-like structures (Fig. 2C). The corresponding AFM image shows that the dots at the sides of the chains correspond to upright TNPs, as indicated by the red arrows and oval in Fig. 2D, and we also observed many dots within the chain structure. Recalling the chemical structure of TNP (Fig. 1A), we can assign six dots as the hydrogen atoms in the side-lying TNP, as indicated by the yellow arrows and the trigonal-shaped visual guide. Because the height of the side-lying TNPs is shorter than that of the upright TNPs by 140 pm, they appear darker (more negative frequency shift) in constant height mode. Furthermore, even within each side-lying and upright TNP, small corrugations are also observed (fig. S3). Further TNP deposition leads to the formation of films with a 1 × 1 structure of side-lying TNPs, terminating with upright TNPs at the edges (Fig. 2, E and F).

In contrast, no particular self-assembly was seen with TFAP (Fig. 2G), where we mainly observed the formation of dimer configurations. The observed STM topography corrugates more than that of TNP, indicating that the observed TFAP on Ag(111) is upright. The corresponding AFM image shows two bright spots for each TFAP, as indicated by the red arrows and oval (Fig. 2H), where the observed contrast is strongly affected by the tip-sample distance (figs. S4 and S5). In particular, two bright spots, corresponding to the hydrogen atoms, become connected at closer tip-sample distance.

To identify the imaging mechanism, we measured a two-dimensional frequency shift map over TFAP (along I-II in Fig. 3A). The right panel

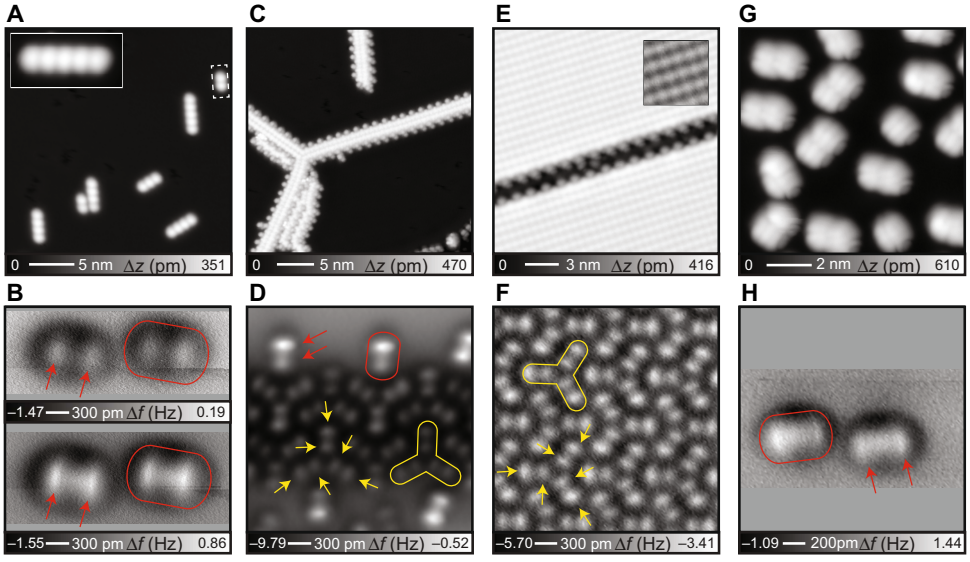

Fig. 2. Experimental observations of TNP and TFAP on Ag(111). (**A** to **F**) Series of STM topographies (A, C, and E) of TNP deposited on the Ag(111) surface with increasing coverage and corresponding AFM images (B, D, and F). As the coverage of TNP increases, the ratio of the upright (red arrows) and side-lying (yellow arrow) TNP becomes larger. (**G**) STM topography of upright TFAP and (**H**) corresponding AFM image. Measurement parameters: For STM observations, tunneling current $I = 1.0$ pA and bias voltage $V = -300$ mV (A), $I = 0.8$ pA and $V = -200$ mV (C), $I = 0.8$ pA and $V = -200$ mV (E), and $I = 0.8$ pA and $V = 500$ mV (G); for AFM observations, oscillation amplitude $A = 60$ pm and $V = 0$ mV (B, D, F, and H).

shows the corresponding AFM image, in which the apparent hydrogen atom spacing (about 300 pm) is larger than the calculated value (246 pm). This larger gap reflects that nature of the tip-surface interaction, as will be discussed below. Figure 3B shows the two-dimensional frequency shift map across two hydrogen atoms, measured with a CO-functionalized tip. At a large tip-sample distance, the frequency shift gradually changes to more negative values with the turning point located at $z = 100$ pm over the hydrogen atom. The gap between the two turning points is approximately 280 pm. The corresponding imaging distance set for the right inset of Fig. 3A is $z = 50$ pm. At small tip-sample separation, no significant contrast between two hydrogen atoms is observed. By integrating the frequency shift along the z direction, a force map was obtained (Fig. 3C and fig. S6). Although the non–site-dependent, long-range tip-substrate interactions were subtracted from the frequency map (Fig. 3B), the site-dependent molecular-tip interactions remain. Therefore, a dark halo representing an attractive force field is seen around the molecule. The most attractive site is located between two hydrogen atoms and has a strength of −40 pN, of similar order to the atomic-scale van der Waals interaction (*31*).

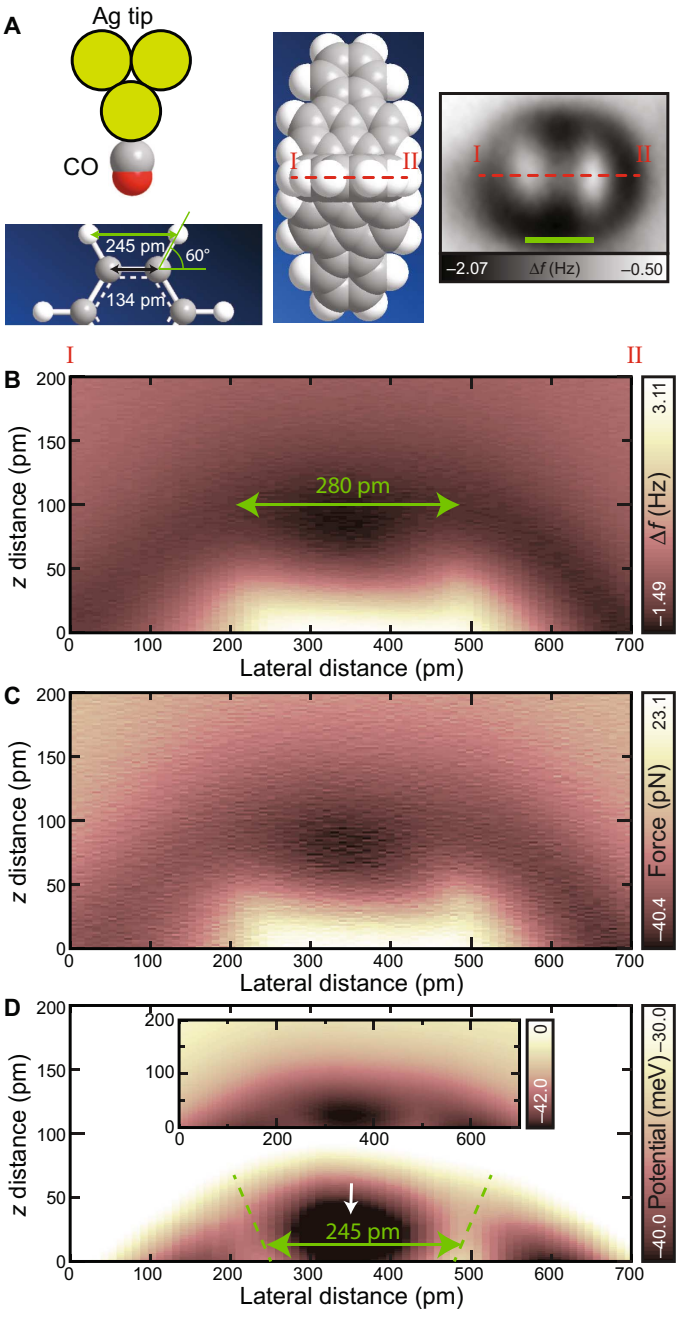

Fig. 3. Quantitative measurements of the C–O···H–C bond. (**A**) Schematic drawing of the hydrogen bonding measurement on TFAP with a CO-functionalized tip. Right shows the AFM image. Scale bar, 300 pm. (**B**) Two-dimensional frequency shift map. (**C**) Calculated force and (**D**) potentials. Inset shows the same area with a wider contrast. The z origin was set at the position of the hydrogen atom. Measurement parameters: $A = 60$ pm and $V = 0$ mV.

To further quantify this interaction, we calculated the potential energy map by integrating the force field (Fig. 3D). A dip of the potential is located at $z = 25$ pm between two C–H bonds. By taking the ridge lines of the potential tails (as indicated by broken green lines), we found that the measured angles (55°) are very close to the chemical model shown in the left inset of Fig. 3A. Furthermore, by taking the defined distance between two hydrogen atoms in TFAP (245 pm), experiments would suggest that the cores of the hydrogen atoms are located at about $z = 25$ pm. However, the onset of strong repulsion with the hydrogen cores means that this is unlikely and the real distance, and observed angle, is a convolution with the tip interaction and deflection, as the theory will show.

To understand the nature of the tip-surface interaction and hydrogen imaging, we performed extensive theoretical calculations of the same molecular system including a CO-functionalized metallic tip. To check the general imaging observed in Fig. 2, we performed simple mechanical AFM modeling (*28*) and obtained very similar images of upright and side-lying TNP and TFAP, confirming the configuration of the molecules on the surface (figs. S7 and S8). Taking into account the general issues around image interpretation with CO-functionalized tips (*27*, *28*), we also artificially removed peripheral hydrogens from the molecules, resulting in qualitatively different images (fig. S9) and emphasizing that we are seeing hydrogens rather than just the general molecular topography.

Following this, we used DFT simulations to calculate a total energy map as a function of tip position in a plane through the two hydrogens at the top of the upright TFAP configuration. Figure 4A shows the complete data set, and we immediately see features in the short-range region (less than 100 pm) that are absent from the experimental results shown in Fig. 3D. However, if we take into account that the tip height is unknown in the experiment, we can find a region that compares very well with the experimental energy plot. This is shown in Fig. 4B, demonstrating qualitative agreement with Fig. 3D in terms of potential ranges and also showing a potential well of 35 meV, in agreement with the experimental measurement of about 40 meV (inset of Fig. 3D). This also demonstrates that, at the minimum, the tip is a lot further from the molecule than what is suggested by the experiments (hydrogens are at 300 pm from the tip at the minimum). In addition, the predicted angle of (55°) is related to the interaction, not to the C–H bond angle.

If we focus on the energy minimum, we can see that it exists at a distance of about 300 pm between the oxygen on the tip and the hydrogens in the molecule. The distance and energy magnitude would be characteristic of a very weak hydrogen bond (*32*), and analysis of Fig. 4D shows that, as expected, there is no significant electron density between O···H. Calculating the differential charge density by subtracting the density of the isolated tip and molecule from the total system, Fig. 4E shows that there is a small charge transfer from the oxygen at the tip apex into the rest of the tip at the minimum. Note here that the asymmetry is due to the left hydrogen being 20-pm closer to the oxygen

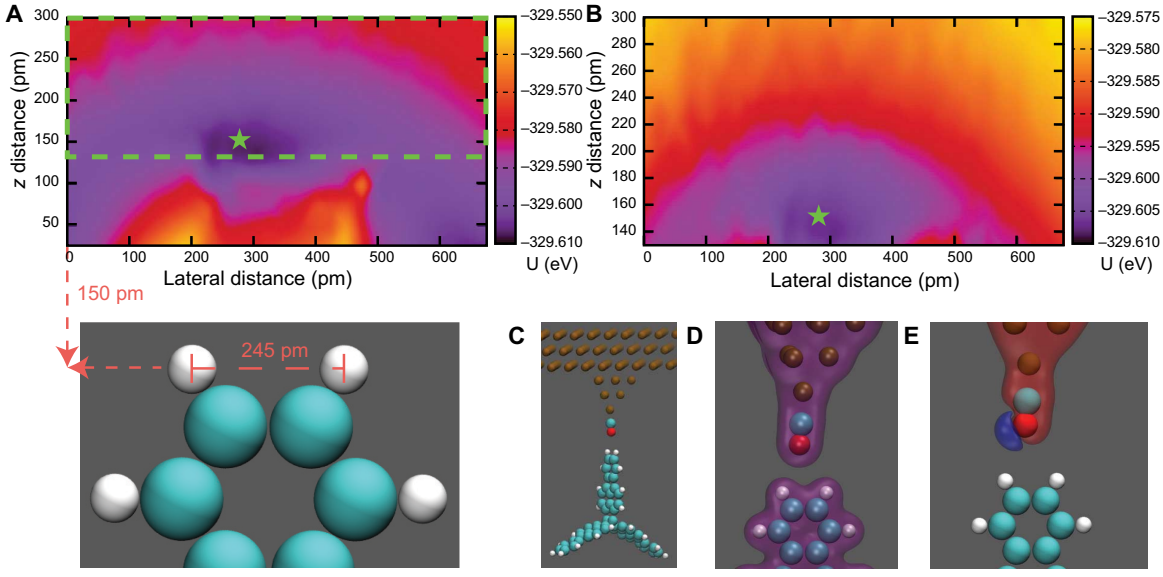

Fig. 4. Simulated results on the TFAP molecule. (**A**) Calculated total energy plot as a function of tip position over the molecule. The molecular structure in the bottom panel is at the height included in the simulation setup, such that the energies plotted along the *x* axis are at 150 pm from the hydrogen atoms. (**B**) Zoomed-in image of the area shown by a dashed green line in (A), where the green star shows the lowest energy position used in the other three images. (**C**) Snapshot of the system configuration. (**D**) Calculated charge density at a contour of 0.05 eV·Å^{-1}. (**E**) Differential charge density at contours of −0.05 (red) and 0.05 eV·Å^{-1} (blue).

and that a mirror image would be obtained moving the tip along the *x* axis closer to the right hydrogen. In this minimum, the nonlinear bond angle agrees with previous studies of C–H···O bonds, favoring nonlinear configurations and suggesting that it is not van der Waals interaction alone (*33*), although much finer sampling would be needed to estimate the angle accurately [for TNP, where the C–H bond is vertical, calculations show differences in the type of differential charge density to TFAP for a similar configuration, supporting this analysis (fig. S10)]. The study of the charge state and electrostatic potential shows that the CO tip has the expected complex interplay of the Smoluchowski effect–induced positive dipole from the metal tip and the negative charge accumulation in front of the oxygen atom due to its lone pair (*34*). This combination interacting with the very weakly charged hydrogens results in the weak attraction in this regime, with the O···H interaction dominating. At longer range, the lack of polarity in TFAP means that the interaction is basically zero once the long-range van der Waals is removed. Reducing the tip-surface distance beyond this point soon results in entering the strongly repulsive region, and we observe significant deflections of the CO at the tip apex (fig. S11).

DISCUSSION

In summary, we have shown that high-resolution AFM with a CO-functionalized tip can resolve the outmost hydrogen atoms of single molecules directly via the O···H–C intermolecular interaction. This very weak interaction, caused just before the onset of Pauli repulsion, is responsible for the spatially localized contrast of the hydrogen atom and was used as a marker to identify the adsorption geometry of the three-dimensional hydrocarbon. Potentially, this technique can be expanded for identifications of more complex large molecules such as DNAs and polymers. Furthermore, here, we used a linear O···H–C system for the direct detection of the intermolecular interaction. This geometry, in principle, allows us to investigate any kind of intermolecular interactions in a quantitative manner at the atomic scale.

MATERIALS AND METHODS

Experimental

All experiments were performed with the Omicron STM/AFM with a qPlus configuration (*35*), operating at 4.8 K in ultrahigh vacuum. A clean Ag(111) surface was prepared in situ by repeated cycles of standard sputtering and annealing. The W tip of a tuning fork sensor was sharpened ex situ by focused ion beam milling and was then covered in situ with Ag atoms by contacting to the sample surface. TNP (*30*) and TFAP (*30*) were deposited on Ag(111) surfaces from a crucible of Knudsen cell, resistively heated at 160° and 230°C, respectively. The resonance frequency of the self-oscillating qPlus sensor was detected by a digital lock-in amplifier (Nanonis OC4 and Zurich Instruments HF2LI-PLL). In STM mode, the tip was biased, whereas the sample was electronically grounded. The topographic images were taken in a constant current mode. In AFM mode, the tip apex was terminated by a CO molecule (*16*), and all images were taken at a constant height mode.

Theoretical calculations

All first principles calculations in this work were performed using the periodic plane-wave basis VASP (Vienna ab initio simulation package) code (*36*, *37*) implementing the spin-polarized DFT. To accurately include van der Waals interactions in this system, we used the optB86B + vdW-DF functional, selected on the basis of a previous work showing that it provides a sufficiently accurate description for all subsystems involved in the measurement (*38*–*40*). Projected augmented wave potentials were used to describe the core electrons (*41*), with a kinetic energy cutoff of 550 eV (with PREC = accurate). Systematic *k*-point convergence was checked for all systems, with sampling chosen according to system size and the gamma point being used for the final production run. This approach converged the total energy of all the systems to the order of a millielectron volt. The properties of the bulk and surface of copper, CO adsorption on copper, and the isolated molecular structure, were carefully checked within this methodology, and

agreement was achieved with the experiments. Bader charge analysis was used to estimate charge transfer in the simulations (*42*).

The tip model consisted of a 10-atom pyramid cluster adsorbed onto a periodic (111) three-layer copper surface slab (see fig. S10). This model was chosen after an extensive study into possible CO-metallic tip structures (to be published separately), which showed that the most stable and representative tip models include a surface above the sharp apex—the proximity of several sharp apices on isolated metallic clusters usually produced unrepresentative interactions due to the cumulative Smoluchowski effect (*43*). This tip was then scanned over the isolated molecule in the *xz* plane, calculating the relaxed total energy in a grid of about 250 points. In these simulations, the force tolerance was 0.01 eV·Å^{-1}, with the top three layers of the tip and the bottom half of the molecule kept frozen. For the final energy plot shown here, this grid was interpolated to an order of magnitude increase in fineness to smooth out the data. In these calculations, we made two assumptions: (i) the substrate under the molecule contributes only to long-range forces and can be ignored and (ii) a CO-functionalized copper tip captures the key properties of a CO-functionalized silver tip. For these assumptions, the quantitative agreement with experiments seems to justify their use.

Calculated AFM image

Here, we used the model developed by Hapala *et al.* (*28*) and extended it by adding electrostatic interactions on top of the van der Waals interactions. The molecular structure was taken from the DFT simulations, and the charges were extracted from the DFT calculations via Bader charge analysis (*42*). The mechanical AFM model relied on empirical Lennard-Jones parameters, which were taken from the CHARMM force field (*44*). All other parameters were the same as intended by Hapala *et al.*, and the simulated AFM scan was performed at a resolution of 2.5 pm (in all directions), with a force tolerance criterion of 4×10^{-6} eV·Å^{-1}. The three-dimensional force field was subsequently converted into a frequency shift image (*45*) using the experimental parameters ($f = 23$ kHz, $A = 60$ pm, and $k = 1800$ Nm^{-1}).

SUPPLEMENTARY MATERIALS

Supplementary material for this article is available at http://advances.sciencemag.org/cgi/content/full/3/5/e1603258/DC1

fig. S1. STM topography of standing TNP molecules.
fig. S2. Electrostatic potential surface maps.
fig. S3. Force spectroscopy of TNP.
fig. S4. AFM images of TNP.
fig. S5. AFM images of TFAP.
fig. S6. Detailed explanation of force spectroscopy.
fig. S7. Simulated AFM images of TNP and TFAP.
fig. S8. Simulated AFM images of upright TFAP.
fig. S9. Simulated AFM images of side-lying TNP.
fig. S10. Atomistic snapshots of the tip-surface system.
fig. S11. Simulated results on the upright TNP molecule.
References (*46*, *47*)

REFERENCES AND NOTES

1. A. Bleloch, A. Lupini, Imaging at the picoscale. *Mater. Today* **7**, 42–48 (2004).
2. R. Ishikawa, E. Okunishi, H. Sawada, Y. Kondo, F. Hosokawa, E. Abe, Direct imaging of hydrogen-atom columns in a crystal by annular bright-field electron microscopy. *Nat. Mater.* **10**, 278–281 (2011).
3. K. Harano, T. Homma, Y. Niimi, M. Koshino, K. Suenaga, L. Leibler, E. Nakamura, Heterogeneous nucleation of organic crystals mediated by single-molecule templates. *Nat. Mater.* **11**, 877–881 (2012).
4. J. J. Boland, Role of bond-strain in the chemistry of hydrogen on the Si(100) surface. *Surf. Sci.* **261**, 17–28 (1992).
5. A. Zhao, Q. Li, L. Chen, H. Xiang, W. Wang, S. Pan, B. Wang, X. Xiao, J. Yang, J. G. Hou, Q. Zhu, Controlling the Kondo effect of an adsorbed magnetic ion through its chemical bonding. *Science* **309**, 1542–1544 (2005).
6. P. Liljeroth, J. Repp, G. Meyer, Current-induced hydrogen tautomerization and conductance switching of naphthalocyanine molecules. *Science* **317**, 1203–1206 (2007).
7. T. Kumagai, A. Shiotari, H. Okuyama, S. Hatta, T. Aruga, I. Hamada, T. Frederiksen, H. Ueba, H-atom relay reactions in real space. *Nat. Mater.* **11**, 167–172 (2012).
8. L. Talirz, H. Söde, J. Cai, P. Ruffieux, S. Blankenburg, R. Jafaar, R. Berger, X. Feng, K. Müllen, D. Passerone, R. Fasel, C. A. Pignedoli, Termini of bottom-up fabricated graphene nanoribbons. *J. Am. Chem. Soc.* **135**, 2060–2063 (2013).
9. M. Corso, M. Ondráček, C. Lotze, P. Hapala, K. J. Franke, P. Jelínek, J. I. Pascual, Charge redistribution and transport in molecular contacts. *Phys. Rev. Lett.* **115**, 136101 (2015).
10. C. Lin, Y. Feng, Y. Xiao, M. Dürr, X. Huang, X. Xu, R. Zhao, E. Wang, X.-Z. Li, Z. Hu, Direct observation of ordered configurations of hydrogen adatoms on graphene. *Nano Lett.* **15**, 903–908 (2015).
11. S. Kawai, S. Saito, S. Osumi, S. Yamaguchi, A. S. Foster, P. Spijker, E. Meyer, Atomically controlled substitutional boron-doping of graphene nanoribbons. *Nat. Commun.* **6**, 8098 (2015).
12. L. J. Lauhon, W. Ho, Direct observation of the quantum tunneling of single hydrogen atoms with a scanning tunneling microscope. *Phys. Rev. Lett.* **85**, 4566–4569 (2000).
13. H. González-Herrero, J. M. Gómez-Rodríguez, P. Mallet, M. Moaied, J. J. Palacios, C. Salgado, M. M. Ugeda, J.-Y. Veuillen, F. Yndurain, I. Brihuega, Atomic-scale control of graphene magnetism by using hydrogen atoms. *Science* **352**, 437–441 (2016).
14. M. A. Lantz, H. J. Hug, R. Hoffmann, P. J. A. van Schendel, P. Kappenberger, S. Martin, A. Baratoff, H.-J. Güntherodt, Quantitative measurement of short-range chemical bonding forces. *Science* **291**, 2580–2583 (2001).
15. Y. Sugimoto, P. Pou, M. Abe, P. Jelinek, R. Pérez, S. Morita, Ó. Custance, Chemical identification of individual surface atoms by atomic force microscopy. *Nature* **446**, 64–67 (2007).
16. L. Gross, F. Mohn, N. Moll, P. Liljeroth, G. Meyer, The chemical structure of a molecule resolved by atomic force microscopy. *Science* **325**, 1110–1114 (2009).
17. N. Moll, L. Gross, F. Mohn, A. Curioni, G. Meyer, The mechanisms underlying the enhanced resolution of atomic force microscopy with functionalized tips. *New J. Phys.* **12**, 125020 (2010).
18. F. Albrecht, N. Pavliček, C. Herranz-Lancho, M. Ruben, J. Repp, Characterization of a surface reaction by means of atomic force microscopy. *J. Am. Chem. Soc.* **137**, 7424–7428 (2015).
19. B. Schuler, G. Meyer, D. Peña, O. C. Mullins, L. Gross, Unraveling the molecular structures of asphaltenes by atomic force microscopy. *J. Am. Chem. Soc.* **137**, 9870–9876 (2015).
20. N. Pavliček, B. Schuler, S. Collazos, N. Moll, D. Pérez, E. Guitián, G. Meyer, D. Peña, L. Gross, On-surface generation and imaging of arynes by atomic force microscopy. *Nat. Chem.* **7**, 623–628 (2015).
21. S. Kawai, V. Haapasilta, B. D. Lindner, K. Tahara, P. Spijker, J. A. Buitendijk, R. Pawlak, T. Meier, Y. Tobe, A. S. Foster, E. Meyer, Thermal control of sequential on-surface transformation of a hydrocarbon molecule on a copper surface. *Nat. Commun.* **7**, 12711 (2016).
22. N. Kocić, X. Liu, S. Chen, S. Decurtins, O. Krejčí, P. Jelínek, J. Repp, S.-X. Liu, Control of reactivity and regioselectivity for on-surface dehydrogenative aryl–aryl bond formation. *J. Am. Chem. Soc.* **138**, 5585–5593 (2016).
23. S. Kawai, A. Sadeghi, X. Feng, P. Lifen, R. Pawlak, T. Glatzel, A. Willand, A. Orita, J. Otera, S. Goedecker, E. Meyer, Obtaining detailed structural information about supramolecular systems on surfaces by combining high-resolution force microscopy with ab initio calculations. *ACS Nano* **7**, 9098–9105 (2013).
24. N. Moll, B. Schuler, S. Kawai, F. Xu, L. Peng, A. Orita, J. Otera, A. Curioni, M. Neu, J. Repp, G. Meyer, L. Gross, Image distortions of a partially fluorinated hydrocarbon molecule in atomic force microscopy with carbon monoxide terminated tips. *Nano Lett.* **14**, 6127–6131 (2014).
25. S. Kawai, A. Sadeghi, F. Xu, L. Peng, A. Orita, J. Otera, S. Goedecker, E. Meyer, Extended halogen bonding between fully fluorinated aromatic molecules. *ACS Nano* **9**, 2574–2583 (2015).
26. L. Gross, F. Mohn, N. Moll, B. Schuler, A. Criado, E. Guitián, D. Peña, A. Gourdon, G. Meyer, Bond-order discrimination by atomic force microscopy. *Science* **337**, 1326–1329 (2012).
27. S. K. Hämäläinen, N. van der Heijden, J. van der Lit, S. den Hartog, P. Liljeroth, I. Swart, Intermolecular contrast in atomic force microscopy images without intermolecular bonds. *Phys. Rev. Lett.* **113**, 186102 (2014).
28. P. Hapala, G. Kichin, C. Wagner, F. S. Tautz, R. Temirov, P. Jelínek, Mechanism of high-resolution STM/AFM imaging with functionalized tips. *Phys. Rev. B* **90**, 085421 (2014).

29. G. Dyker, J. Körning, P. G. Jones, P. Bubenitschek, Palladium-catalyzed arylation of tetrasubstituted double bonds: A simple synthesis of annelated propellanes. *Angew. Chem. Int. Ed. Engl.* **32**, 1733–1735 (1993).
30. T. Kubo, S. Miyazaki, T. Kodama, M. Aoba, Y. Hirao, H. Kurata, A facile synthesis of trinaphtho[3.3.3]propellane and its π-extension and the formation of a two-dimensional honeycomb molecular assembly. *Chem. Commun.* **51**, 3801–3803 (2015).
31. S. Kawai, A. S. Foster, T. Björkman, S. Nowakowska, J. Björk, F. F. Canova, L. H. Gade, T. A. Jung, E. Meyer, Van der Waals interactions and the limits of isolated atom models at interfaces. *Nat. Commun.* **7**, 11559 (2016).
32. P. A. Kollman, L. C. Allen, Theory of the hydrogen bond. *Chem. Rev.* **72**, 283–303 (1972).
33. D. Ž. Veljković, G. V. Janjić, S. D. Zarić, Are C–H···O interactions linear? The case of aromatic CH donors. *CrystEngComm* **13**, 5005–5010 (2011).
34. M. Ellner, N. Pavliček, P. Pou, B. Schuler, N. Moll, G. Meyer, L. Gross, R. Peréz, The electric field of CO tips and its relevance for atomic force microscopy. *Nano Lett.* **16**, 1974–1980 (2016).
35. F. J. Giessibl, High-speed force sensor for force microscopy and profilometry utilizing a quartz tuning fork. *Appl. Phys. Lett.* **73**, 3956–3958 (1999).
36. G. Kresse, J. Furthmüller, Efficiency of ab-initio total energy calculations for metals and semiconductors using a plane-wave basis set. *Comput. Mater. Sci.* **6**, 15–50 (1996).
37. G. Kresse, J. Furthmüller, Efficient iterative schemes for ab initio total-energy calculations using a plane-wave basis set. *Phys. Rev. B* **54**, 11169–11186 (1996).
38. J. Klimeš, D. R. Bowler, A. Michaelides, Chemical accuracy for the van der Waals density functional. *J. Phys. Condens. Matter* **22**, 022201 (2010).
39. J. Klimeš, D. R. Bowler, A. Michaelides, Van der Waals density functionals applied to solids. *Phys. Rev. B* **83**, 195131 (2011).
40. T. Björkman, A. Gulans, A. V. Krasheninnikov, R. M. Nieminen, Van der Waals bonding in layered compounds from advanced density-functional first-principles calculations. *Phys. Rev. Lett.* **108**, 235502 (2012).
41. P. E. Blöchl, Projector augmented-wave method. *Phys. Rev. B* **50**, 17953–17979 (1994).
42. W. Tang, E. Sanville, G. Henkelman, A grid-based Bader analysis algorithm without lattice bias. *J. Phys. Condens. Matter* **21**, 084204 (2009).
43. D. Z. Gao, J. Grenz, M. B. Watkins, F. F. Canova, A. Schwarz, R. Wiesendanger, A. L. Shluger, Using metallic noncontact atomic force microscope tips for imaging insulators and polar molecules: Tip characterization and imaging mechanisms. *ACS Nano* **8**, 5339–5351 (2014).
44. B. R. Brooks, C. L. Brooks III, A. D. Mackerell Jr., L. Nilsson, R. J. Petrella, B. Roux, Y. Won, G. Archontis, C. Bartels, S. Boresch, A. Caisch, L. Caves, Q. Cui, A. R. Dinner, M. Feig, S. Fischer, J. Gao, M. Hodoscek, W. Im, K. Kuczera, T. Lazaridis, J. Ma, V. Ovchinnikov, E. Paci, R. W. Pastor, C. B. Post, J. Z. Pu, M. Schaefer, B. Tidor, R. M. Venable, H. L. Woodcock, X. Wu, W. Yang, D. M. York, M. Karplus, CHARMM: The biomolecular simulation program. *J. Comput. Chem.* **30**, 1545–1614 (2009).
45. J. Welker, E. Illek, F. J. Giessibl, Analysis of force-deconvolution methods in frequency-modulation atomic force microscopy. *Beilstein J. Nanotechnol.* **3**, 238–248 (2012).
46. M. J. Frisch, G. W. Trucks, H. B. Schlegel, G. E. Scuseria, M. A. Robb, J. R. Cheeseman, J. A. Montgomery Jr., T. Vreven, K. N. Kudin, J. C. Burant, J. M. Millam, S. S. Iyengar, J. Tomasi, V. Barone, B. Mennucci, M. Cossi, G. Scalmani, N. Rega, G. A. Petersson, H. Nakatsuji, M. Hada, M. Ehara, K. Toyota, R. Fukuda, J. Hasegawa, M. Ishida, T. Nakajima, Y. Honda, O. Kitao, H. Nakai, M. Klene, X. Li, J. E. Knox, H. P. Hratchian, J. B. Cross, V. Bakken, C. Adamo, J. Jaramillo, R. Gomperts, R. E. Stratmann, O. Yazyev, A. J. Austin, R. Cammi, C. Pomelli, J. W. Ochterski, P. Y. Ayala, K. Morokuma, G. A. Voth, P. Salvador, J. J. Dannenberg, V. G. Zakrzewski, S. Dapprich, A. D. Daniels, M. C. Strain, O. Farkas, D. K. Malick, A. D. Rabuck, K. Raghavachari, J. B. Foresman, J. V. Ortiz, Q. Cui, A. G. Baboul, S. Cliord, J. Cioslowski, B. B. Stefanov, G. Liu, A. Liashenko, P. Piskorz, I. Komaromi, R. L. Martin, D. J. Fox, T. Keith, M. A. Al-Laham, C. Y. Peng, A. Nanayakkara, M. Challacombe, P. M. W. Gill, B. Johnson, W. Chen, M. W. Wong, C. Gonzalez, J. A. Pople, *Gaussian 03, Revision C.02* (Gaussian Inc., 2004).
47. B. Schuler, W. Liu, A. Tkatchenko, N. Moll, G. Meyer, A. Mistry, D. Fox, L. Gross, Adsorption geometry determination of single molecules by atomic force microscopy. *Phys. Rev. Lett.* **111**, 106103 (2013).

Acknowledgments: P.S., J.T., and A.S.F. acknowledge the use of the Centre for Scientific Computing, Helsinki for computational resources. **Funding:** This work was supported, in part, by the Japan Science and Technology Agency Precursory Research for Embryonic Science and Technology for the project "Molecular technology and creation of new functions," by the Japan Society for the Promotion of Science (KAKENHI grant nos. 15K21765 and JP16K14064), by the Swiss National Science Foundation, by the Swiss Nanoscience Institute, and by COST (European Cooperation in Science and Technology) action MP1303 "Understanding and controlling nano and mesoscale friction." A.S.F. was supported by the Academy of Finland through its Centres of Excellence Program (project no. 915804) and European Union project PAMS (contract no. 610446). **Author contributions:** S.K. conducted the experiments and carried out the data analysis. T.N., T. Kodama, and T. Kubo synthesized the precursor molecule. A.S.F., P.S., and J.T. conducted theoretical calculations. S.K., A.S.F., P.S., and E.M. contributed to writing of the manuscript. All authors commented on the manuscript. S.K. and T.N. planned the project. **Competing interests:** The authors declare that they have no competing interests. **Data and materials availability:** All data needed to evaluate the conclusions in the paper are present in the paper and/or the Supplementary Materials. Additional data related to this paper may be requested from the authors.

Submitted 22 December 2016
Accepted 14 March 2017
Published 12 May 2017
10.1126/sciadv.1603258

Citation: S. Kawai, T. Nishiuchi, T. Kodama, P. Spijker, R. Pawlak, T. Meier, J. Tracey, T. Kubo, E. Meyer, A. S. Foster, Direct quantitative measurement of the C═O···H–C bond by atomic force microscopy. *Sci. Adv.* **3**, e1603258 (2017).

Science Advances

Direct quantitative measurement of the C?O···H–C bond by atomic force microscopy

Shigeki Kawai, Tomohiko Nishiuchi, Takuya Kodama, Peter Spijker, Rémy Pawlak, Tobias Meier, John Tracey, Takashi Kubo, Ernst Meyer and Adam S. Foster

Sci Adv **3** (5), e1603258.
DOI: 10.1126/sciadv.1603258